Research on Variable Direction Wireless Power Transfer System based on Auxiliary Coils: Theory, Simulation and Experimental Verification

Feihang Xiao[1] and Hao Qiang[1,2]

[1]School of Mechanical Engineering and Rail Transit
Changzhou University, Changzhou 213164, China
xiaofeihang2000@163.com, qhao@cczu.edu.cn

[2]Jiangsu Province Engineering Research Center of High-Level Energy and Power Equipment
Changzhou University, Changzhou 213164, China

Abstract – In complex environments such as mines and pipelines, wireless power transfer (WPT) technology stands as a safe and convenient method for supplying power. However, in practical applications, the unavoidable angular misalignment between the sending and receiving coils results in decreased power. To address this issue, this paper proposes a variable direction WPT design method based on auxiliary coils. The mutual inductance of the system is analyzed with coils placed at different positions and incorporating multiple auxiliary coils. This paper conducts simulation and experimental analysis based on a 45° angle between the horizontal shaft and the slant shaft, showing a 14.92% increase in received power. The effectiveness of the proposed design method validates the feasibility of the technology and offers substantial support for practical applications.

Index Terms – Codirectional coil, variable direction coil, variable direction transfer, wireless power transfer.

I. INTRODUCTION

Wireless power transfer (WPT) technology has lately gained increasing attention as an alternative way to transfer power with respect to a cabled connection [1]. Due to its advantages of high reliability [2], safety [3], flexible usage [4], low maintenance cost [5] and better adaptability in some extreme or special conditions [6, 7], it is widely used in various fields, including internet of things [8], electric vehicles [9], medical devices [10], etc.

In 2007, MIT successfully illuminated a 60 W bulb one meter away using magnetic field resonance [11]. Magnetic coupled resonant wireless power transfer (MCR-WPT) has emerged as the most promising medium-distance wireless transfer mode.

Coupling coils are a key part of a WPT system [12]. Currently, the majority of WPT systems impose strict requirements on the coil's positioning during operation. Misalignment between the sending and receiving coils significantly reduces received power [13].

In certain application scenarios, coil placement is restricted, preventing direct alignment. As shown in Fig. 1, in the mining industry, the sending coil on the mining car moves with the slant shaft, while the receiving coil is positioned on the wellbore. When the mining car supplies power to electrical equipment on the slant shaft, direct alignment is possible. However, when powering equipment on the horizontal shaft, an angle between the sending and receiving coils reduces received power [14].

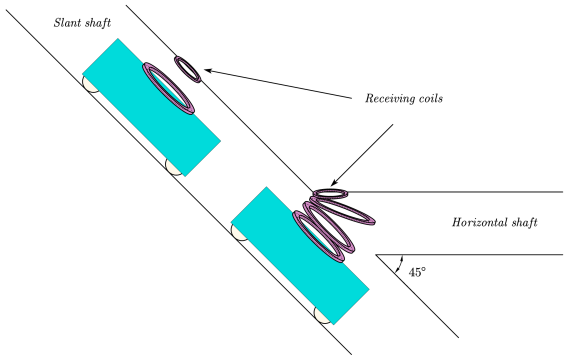

Fig. 1. Schematic of the location of WPT coils in coal mines.

To enhance coil transfer efficiency in diverse scenarios, [15] introduced ferrite between the sending and receiving ends to increase the transfer power when misaligned. However, maintaining consistent shapes for the sending and receiving coils is necessary. By winding Litz lines at different positions on the ferrite, [16] altered the magnetic field distribution, providing improved resistance to misalignment.

To supply power to receiving coils at various angles, [17] utilizes multiple relay coils for equipment power,

Submitted On: January 13, 2024
Accepted On: June 18, 2024

1054-4887 © ACES

https://doi.org/10.13052/2024.ACES.J.390408

but requiring separate capacitors to be configured for each coil. Although multi degree of freedom WPT technology energizes devices at different positions and angles, its structure is generally complex and demands sophisticated control methods [18].

Due to the angular misalignment between the sending coil and the receiving coil, the distribution of the electromagnetic field and the process of power transfer become complex. Therefore, based on electromagnetic field analysis and finite element simulation, a design method for a variable direction WPT system was proposed. Through mutual inductance calculation and simulation, the case of a horizontal shaft and a slant shaft with an angle of 45° was analyzed. The proposed method is applicable for cases where the angle is less than 90°. The main contributions of this paper are as follows:

(1) This paper analyzes the mutual inductance between multiple coils and the occurrence of angular errors between coils.
(2) A design method for variable direction WPT based on auxiliary coils was proposed.
(3) The experimental prototype is designed to measure the power transfer of different numbers of auxiliary coils and auxiliary coils at different positions. With the proposed design method, the received power can be increased by 14.92%.

II. THEORETICAL ANALYSIS

A. Basic WPT analysis

The equivalent circuit method was utilized to model the WPT system in our research. The equivalent circuit method simplifies complex electromagnetic systems into circuit models for analysis, providing an intuitive description of the power conversion and transfer processes among system components.

The MCR-WPT system mainly consists of a high-frequency (HF) power supply, sending module (sending coil), receiving module (receiving coil) and load [12, 19]. The equivalent circuit is depicted in Fig. 2.

R_{AC} represents the equivalent impedance of the HF power supply AC. L_S, C_S and R_{LS} denote the equivalent inductance, resonant capacitance and equivalent resistance of the sending module. Similarly, L_R, C_R and R_{LR} represent the equivalent inductance, resonant capacitance and equivalent resistance of the receiving module. R_L signifies the load resistance, while M_{SR} stands for the mutual inductance between the two coils. In accordance with Fig. 2, deducing the Kirchhoff's Voltage Law (KVL) equations of the two circuits with the operating angular frequency ω is straightforward:

$$\begin{bmatrix} Z_S & j\omega M_{SR} \\ j\omega M_{SR} & Z_R \end{bmatrix} \begin{bmatrix} \dot{I}_S \\ \dot{I}_R \end{bmatrix} = \begin{bmatrix} \dot{U}_{AC} \\ 0 \end{bmatrix}. \tag{1}$$

$\dot{I}_S$ and $\dot{I}_R$ are the currents of the sending circuit and the receiving circuit, $\dot{U}_{AC}$ is the input voltage and P_L is the power of load. The transfer efficiency η is defined as the ratio of load power to input power. Z_S and Z_R represent the equivalent impedance of the sending coil circuit and the receiving coil circuit, respectively. When resonance occurs between the sending and receiving coils, the load power P_L and efficiency η are highest:

$$\eta = \frac{P_L}{\dot{U}_{AC}\dot{I}_S} \times 100\% = \frac{\dot{I}_R^2 R_L}{\dot{U}_{AC}\dot{I}_S} \times 100\%. \tag{2}$$

In the MCR-WPT system, the coupling coefficient k represents the coupling strength between two coils, defined as follows:

$$k = \frac{M_{SR}}{\sqrt{L_S L_R}}. \tag{3}$$

According to the definition of coupling coefficient, the mutual inductance directly determines the coil coupling strength when the coil parameters are fixed. Therefore, mutual inductance is key to analyzing the transfer capacity of WPT systems.

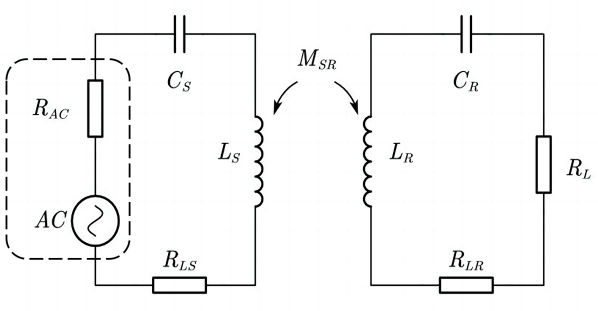

Fig. 2. Equivalent circuit of MCR-WPT system.

B. Variable direction WPT analysis

In WPT systems, power is transmitted from the transmitter module to the receiving module through electromagnetic field coupling, where mutual inductance serves as a crucial parameter to describe this coupling strength [20]. When dealing with complex electromagnetic systems, the simple equivalent circuit method may not provide sufficiently accurate analysis results. To calculate the mutual inductance between coils, the Neumann formula from computational electromagnetics was employed for analysis. This method enables precise calculation of mutual inductance between coils at different positions and angles, serving as a reference for system design and optimization.

The coils used in this paper are all coaxial multi-turn circular coils. For ease of observation, they are depicted as single-turn coils in the figures.

Establishing a coordinate system with the center of the sending coil as the origin, the center of the receiving coil remains in the yz plane and shifts towards the

positive y-axis until the outer radius of the receiving coil is tangent to the inner radius of the sending coil. Subsequently, using the tangent point as the center of rotation, a 45° rotation is performed about an axis parallel to the x-axis, directed away from the sending coil. The positional relationship between the sending and receiving coils post-rotation is illustrated in Fig. 3.

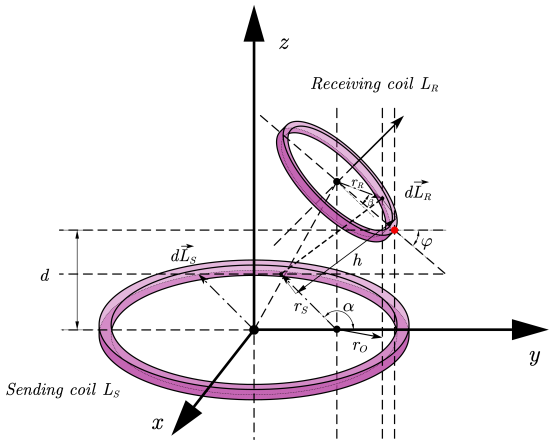

Fig. 3. Schematic of coil position.

The spatial position of the sending coil and the receiving coil undergo changes after rotation, introducing complexity to the calculation of mutual inductance. To simplify the calculation, assuming uniform flow of coil current through the conductor element and neglecting skin effect, mutual inductance can be expressed as [21]:

$$M_{\mathrm{SR}} = \frac{\mu_0 N_S N_R}{4\pi} \oint_{L_S} \oint_{L_R} \frac{d\vec{L_S} \cdot d\vec{L_R}}{h}. \tag{4}$$

μ_0 represents the vacuum magnetic permeability. N_S and N_R are the turns of the sending coil and receiving coil, respectively. Based on the proposed equivalent model:

$$d\vec{L_S} \cdot d\vec{L_R} = r_s r_o \cos\alpha \cos\beta, \tag{5}$$

where r_o signifies the length of the projection of the differential element $d\vec{L_R}$ of the receiving coil in the xy plane. Its value depends on the rotation angle φ of the receiving coil and the angular relationship β of the differential element with respect to the point of rotation. Its expression is:

$$r_o = r_R \oint_{L_R} \sqrt{1 + \cos^2\beta \sin^2\varphi}. \tag{6}$$

The airline distance between $d\vec{L_S}$ and $d\vec{L_R}$ is h, derived by:

$$h = \sqrt{(r_R - r_o)^2 + [d_{SR} + r_R(1 - \cos\beta)\sin\varphi]^2}. \tag{7}$$

Compared with the topology before rotation, the coupling between coils is reduced. Auxiliary coils with the same radius as the sending coil can be added between the sending coil and receiving coil to enhance transfer efficiency.

This paper introduces two auxiliary coils, namely the codirectional auxiliary coil L_i and the variable direction auxiliary coil L_j, positioned between the sending and receiving coils. As illustrated in Fig. 4, the codirectional auxiliary coil is placed near the sending coil, aligned coaxially with it. The variable direction auxiliary coil is placed close to the receiving coil, with its axis in the positive half of the yz plane. The angle between the coil plane and xy plane is denoted as θ_n ($\theta_n < \varphi$). The codirectional auxiliary coil enhances the magnetic field intensity, while the variable direction auxiliary coil is designed to alter the direction of magnetic field propagation, facilitating variable direction transfer.

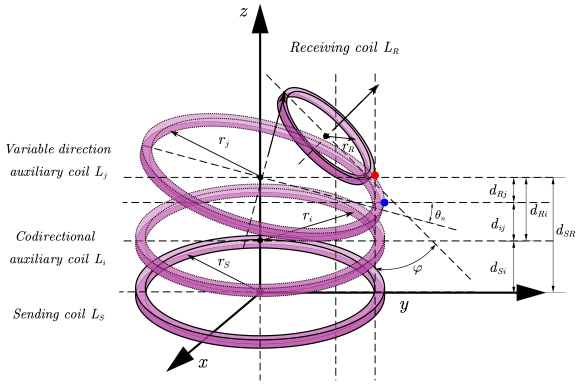

Fig. 4. Schematic of coil position (with auxiliary coils).

d represents the distance between coils, and the two letters after d represent the corresponding coils. For coils with an angle between the xy plane (L_j and L_R), when representing their position with other coils, the point with the highest y-value on the yz plane is used as the reference, as shown by the red and blue dots in Fig. 4.

Both the codirectional auxiliary coil and the variable direction auxiliary coil are multi-turn coils, with subscripts added after the coil name to indicate a particular turn of coil, denoted as L_{i1}, L_{i2}, …, L_{in} and L_{j1}, L_{j2}, …, L_{jn}. According to equation (4), the mutual inductance between each coil can be calculated:

$$M_{Sin} = \frac{\mu_0 N_S N_{in}}{4\pi} \oint_{L_S} \oint_{L_{in}} \frac{r_s^2 \cos\alpha_S d\alpha d\beta_{in}}{\sqrt{2r_s^2(1 - \cos\alpha_S) + d_{Sin}^2}}, \tag{8}$$

$$M_{Sjn}=\frac{\mu_0 N_S N_{jn}}{4\pi}\oint_{L_S}\oint_{L_{jn}}\frac{r_S^2\cos\alpha_S d\alpha_S d\beta_{jn}\oint_{L_{jn}}\sqrt{1-\cos^2\beta_{jn}\sin^2\theta_n}}{\sqrt{\left(r_{jn}-\oint_{L_{j1}}r_{jn}\sqrt{1-\cos^2\beta_{jn}\sin^2\theta_n}\right)^2+\left[d_{sjn}+r_{jn}(1-\cos\beta_{jn})\sin\theta_n\right]^2}},\tag{9}$$

$$M_{Rjn}=\frac{\mu_0 N_{jn} N_R}{4\pi}\oint_{L_{jn}}\oint_{L_R}\frac{r_S\cos\alpha_R d\alpha_R d\beta_{jn}\oint_{L_R}r_{jn}\sqrt{1-\cos^2\beta_{jn}\sin^2(\varphi-\theta_n)}}{\sqrt{\left(r_R-\oint_{L_R}r_R\sqrt{1-\cos^2\beta_{jn}\sin^2(\varphi-\theta_n)}\right)^2+\left[d_{Rjn}+r_R(1-\cos\beta_{jn})\sin(\varphi-\theta_n)\right]^2}},\tag{10}$$

$$M_{Rin}=\frac{\mu_0 N_{in} N_R}{4\pi}\oint_{L_{in}}\oint_{L_R}\frac{r_{in}\cos\alpha_R d\alpha_R d\beta_{in}\oint_{L_R}r_R\sqrt{1-\cos^2\beta_{in}\sin^2\varphi}}{\sqrt{\left(r_R-\oint_{L_R}r_R\sqrt{1-\cos^2\beta_{in}\sin^2\varphi}\right)^2+\left[d_{Rin}+r_R(1-\cos\beta_{in})\sin\varphi\right]^2}}.\tag{11}$$

The wire of the coil has a conductivity of 6×10^7 S/m, and the cross-sectional diameter of the coil wire is 1 mm. The coil L_S has a turn number of 30, while coils L_i, L_j and L_R have turn numbers of 10. The radius of coils L_S, L_i and L_j are 10 cm, and the radius of coil L_R is 5 cm.

The mutual inductance M_{SR} varies with the frequency f (f=$\omega/2\pi$) and can be obtained using the above parameters, as shown in Fig. 5. When f=70 kHz, the mutual inductance is maximum. As φ increases, M_{SR} decreases.

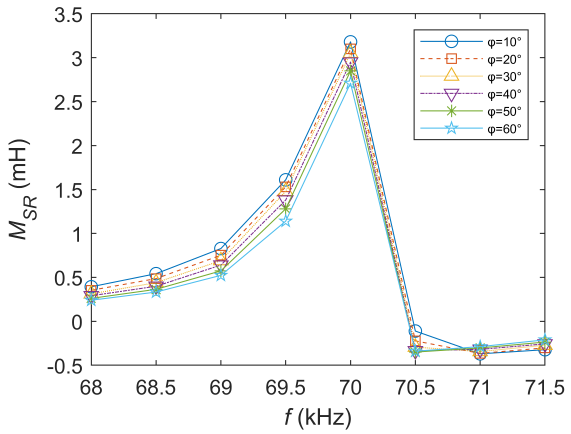

Fig. 5. Curves of M_{SR} varied with f at different φ.

For WPT systems, the maximum power can be realized only at specific angles and distances [22]. Figure 6 illustrates the variation of M_{SR} with respect to f at different d_{Si} when d_{SR}=8 cm. Similarly, when f=70 kHz, the mutual inductance reaches its maximum. It is noteworthy that the maximum value of mutual inductance is obtained at d_{Si}=5 cm.

All auxiliary coils are connected in series with corresponding resonant capacitors C_{in} or C_{jn}, and work resonantly with the system operating frequency. Based on the equivalent circuit model, it is easy to deduce the voltage KVL equations of the system with the operating angular frequency ω:

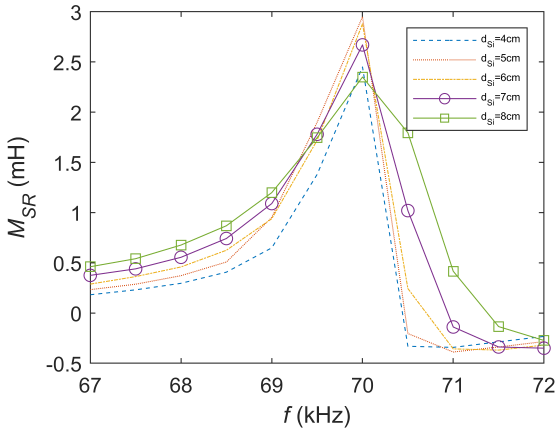

Fig. 6. Curves of M_{SR} varied with f at different d_{Si}.

$$\begin{bmatrix}\dot{I}_S\\ \dot{I}_{i1}\\ \cdots\\ \dot{I}_{j1}\\ \cdots\\ \dot{I}_R\end{bmatrix}\begin{bmatrix}Z_S & j\omega M_{Si1} & \cdots & j\omega M_{Sj1} & \cdots & j\omega M_{SR}\\ j\omega M_{Si1} & Z_{i1} & \cdots & j\omega M_{i1j1} & \cdots & j\omega M_{Ri1}\\ \cdots & j\omega M_{i1i2} & \cdots & \cdots & \cdots & \cdots\\ j\omega M_{Sj1} & \cdots & \cdots & Z_{j1} & \cdots & j\omega M_{Rj1}\\ \cdots & j\omega M_{i1j1} & \cdots & j\omega M_{i1j2} & \cdots & \cdots\\ \cdots & \cdots & \cdots & \cdots & \cdots & \cdots\\ j\omega M_{SR} & j\omega M_{Ri1} & \cdots & j\omega M_{Rj1} & \cdots & Z_R\end{bmatrix}=\begin{bmatrix}\dot{U}_{AC}\\ 0\\ \cdots\\ \cdots\\ \cdots\\ 0\end{bmatrix}.\tag{12}$$

$\dot{I}_S$, $\dot{I}_{in}$, $\dot{I}_{jn}$ and $\dot{I}_R$ represent the currents in the sending circuit, codirectional coil circuit, variable direction coil circuit and receiving circuit, respectively. The total impedance for each circuit is shown in Table 1.

Table 1: Equivalent total impedance of the circuit

Circuit	Total Circuit Impedance
Sending circuit	$Z_S = R_{AC} + \frac{1}{j\omega C_S} + j\omega L_S$
Codirectional coil circuit	$Z_{in} = \frac{1}{j\omega C_{in}} + j\omega L_{in}$
Variable direction coil circuit	$Z_{jn} = \frac{1}{j\omega C_{jn}} + j\omega L_{jn}$
Receiving circuit	$Z_R = R_L + \frac{1}{j\omega C_R} + j\omega L_R$

Furthermore, the current $\dot{I}_R$ in the receiving circuit at various angles of φ and distances d_{Si} can be calculated, which is illustrated in Figs. 7 and 8. Similar to the analysis of mutual inductance, the current reaches its maximum when f=70 kHz, and its magnitude decreases with increasing φ.

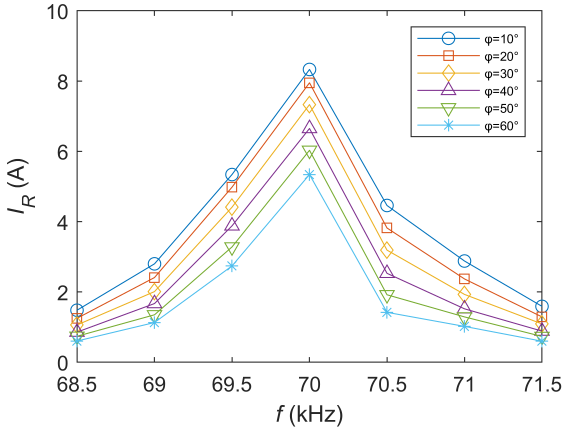

Fig. 7. Curves of $\dot{I}_R$ varied with f at different φ.

As shown in Fig. 8, the current reaches its maximum when d_{Si}=5 cm at a frequency of 70 kHz. The magnitude of the current is directly proportional to the power.

Through mutual inductance calculations, the impact of auxiliary coils on transfer characteristics at different positions and angles was analyzed. The combination of the equivalent circuit method and the Neumann formula provides us with an effective analytical tool, offering essential insights for system design and optimization. Therefore, the addition of auxiliary coils can enhance the magnetic field near the receiving coil from within the geometric structure of the system, thereby improving transfer power.

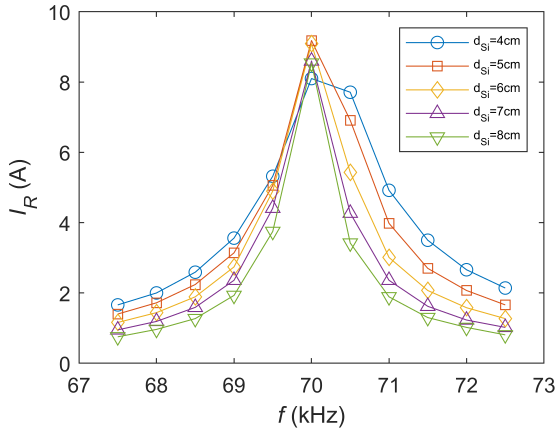

Fig. 8. Curves of $\dot{I}_R$ varied with f at different d_{Si}.

Due to the proposed system having multiple coils and the existence of angular misalignment, there is a lack of explicit formulas to calculate the power. According to equations (1) and (2), mutual inductance and current are key parameters that affect the power transfer. Therefore, feasibility needs to be validated through simulations and experiments.

III. SIMULATION ANALYSIS

A. Design method

After determining the basic structure of the system, it is necessary to further determine the specific positions of the two auxiliary coils. To achieve the maximum received power, the goal can be accomplished through the following steps. The specific process is illustrated in Fig. 9.

The first step involves determining the positions of the sending coil and the receiving coil. The angle between the sending coil and the receiving coil is application-specific, set at 45° in this paper.

In the second step, vary the position of the codirectional auxiliary coil, measure the power received by the receiving coil, and record the maximum power point along with its corresponding position. Moving on to the third step, fix the codirectional auxiliary coil at the identified maximum power point.

In the fourth step, determine the rotation center (blue dot) and axis of the variable direction auxiliary coil. The center position of d_{Ri} on the yz plane is the midpoint, i.e., d_{Rj}=d_{ij}. The rotation axis passes through the rotation center and is parallel to the x-axis.

For the fifth step, rotate the variable direction auxiliary coil around the rotation axis towards the direction of the receiving coil, recording the maximum power point and its corresponding position.

Finally, the sixth step involves fixing the variable direction auxiliary coil at the maximum power point.

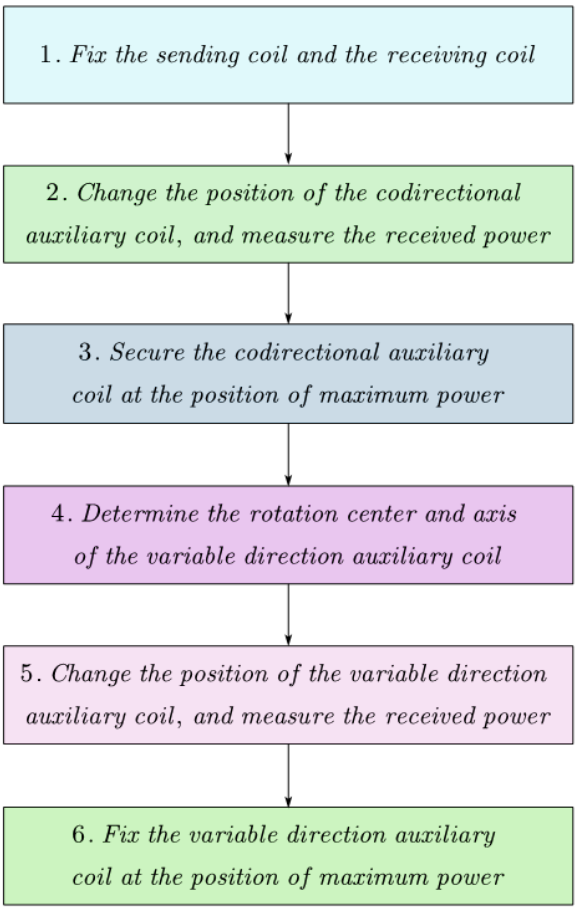

Fig. 9. Variable direction transfer design process.

B. Electromagnetic field simulation

Here we match capacitors according to the coil inductance to construct a resonant circuit. The coil parameters are shown in Table 2.

Table 2: Coil parameters

Coils	Inductance	Series Capacitor	Resistance
Sending coil L_S	170 μH	30 nF	0.422 Ω
Codirectional auxiliary coil L_i	18 μH	30 nF	0.236 Ω
Variable direction auxiliary coil L_j	18 μH	30 nF	0.236 Ω
Receiving coil L_R	170 nH	30 μF	0.15 Ω

The number of turns, radius and other parameters of each coil are consistent with those mentioned earlier.

With a distance d_{SR} of 8 cm between the sending coil and the receiving coil, the position of the codirectional auxiliary coil is altered to measure the system's transfer power at different locations. The measurement results are shown in Fig. 10.

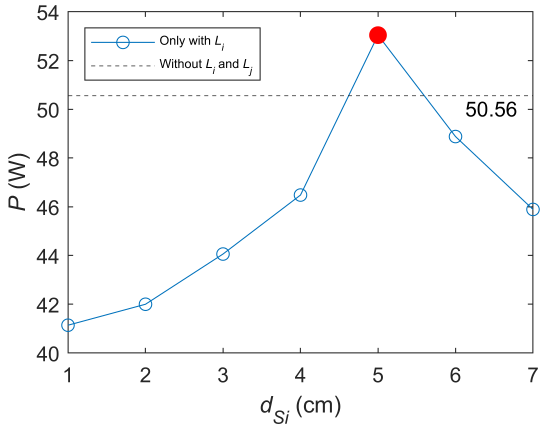

Fig. 10. The received power with codirectional auxiliary coil.

It can be seen that when d_{Si}=5 cm, the transfer power is highest, so the codirectional auxiliary coil is placed in this position. After the addition of the codirectional auxiliary coil, a frequency splitting phenomenon occurred, that is, when the distance between the codirectional auxiliary coil and the sending coil is too close, the power is lower than that without the addition of auxiliary coil [23].

After determining the position of the codirectional auxiliary coil, we studied the impact of the variable direction auxiliary coil. We rotated the axis parallel to the x-axis in the direction away from the sending coil, and measured the transfer power at different angles. The results are shown in Fig. 11.

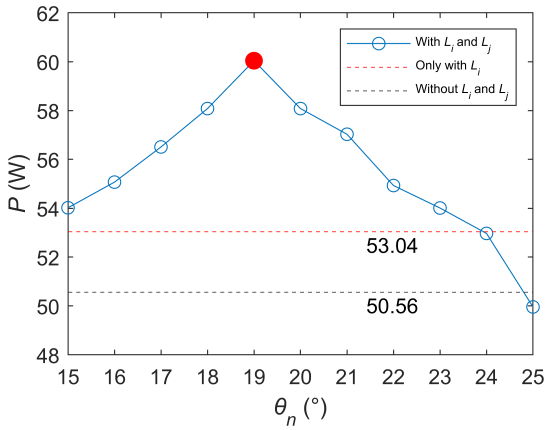

Fig. 11. The received power with two auxiliary coils.

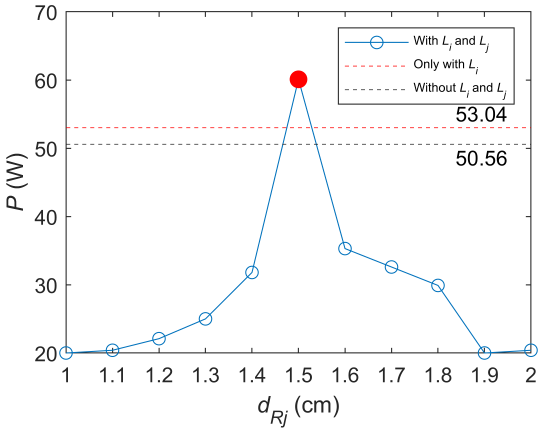

Fig. 12. The received power with two auxiliary coils when θ_n=19°.

When the angle between the variable direction auxiliary coil and the *xy* plane is 19°, the power is maximum and higher than when only the codirectional auxiliary coil is added. Therefore, the proposed design method can effectively improve transfer power and achieve variable direction transfer.

When θ_n is 19°, we varied d_{Rj} and measured the transfer power, as shown in Fig. 12. According to the proposed design method, the rotational center of the variable direction auxiliary coil is located at the center position of d_{Ri}, i.e., d_{Rj}=d_{ij}=1.5 cm. Due to the precise requirements of coil positioning in WPT [22] and the existence of frequency splitting phenomena [23], the power rapidly decreases when the variable direction auxiliary coil is located at other positions.

The magnetic flux distribution of the system is shown in Fig. 13. The magnetic flux generated by the sending coil is guided towards the direction of the receiving coil through the auxiliary coils L_i and L_j, effectively improving the transfer power.

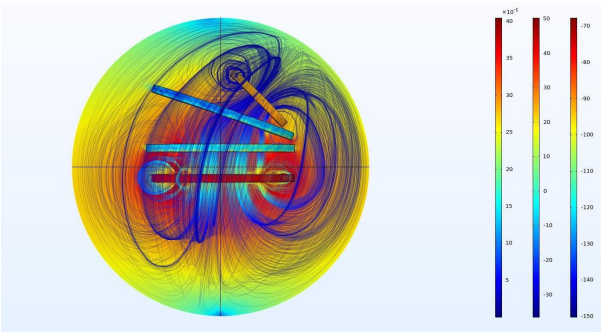

Fig. 13. Magnetic flux distribution.

IV. EXPERIMENTAL MEASUREMENTS AND RESULTS

Analysis from computational electromagnetics provided a basis for studying the placement of auxiliary coils. Validation of the analysis results will be conducted through experiment.

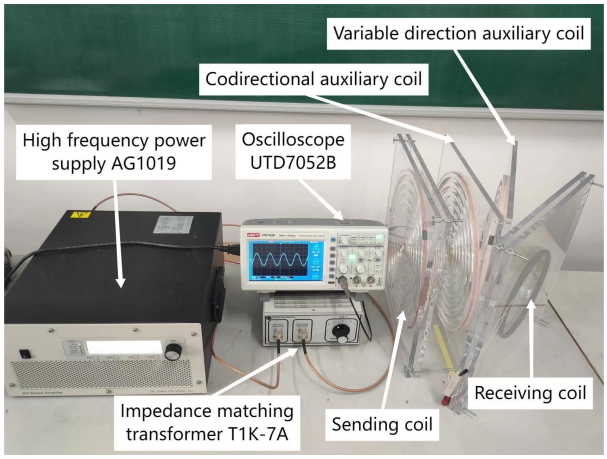

Fig. 14. Experimental prototype.

Figure 14 illustrates the experimental prototype for the variable direction WPT system. Power supply AG1019 is adopted to produce an HF voltage signal with a frequency of 70 kHz. The impedance matching transformer T1K-7A is employed to mitigate the influence of reflected power from the system on AG1019. The parameters of each coil are consistent with those used in the simulation. The experimental prototype adopts an SS topology with a load resistance of 5 Ω.

After fixing the sending and receiving coils, the distance between the codirectional auxiliary coil and the sending coil is varied, and the transfer power is measured at different positions. The results are depicted in Fig. 15.

The power peaks when the distance between the codirectional auxiliary coil and the sending coil is 5 cm. Due to the manual winding of the coil, a slight error in the design size leads to slightly lower experimental power than the simulated power. Specific values measured during the experiment are detailed in Table 3.

To further enhance received power, a variable direction auxiliary coil is added to the system. Following the method described earlier, the codirectional auxiliary coil is fixed at d_{Si}=5 cm. The angle of the variable direction auxiliary coil is adjusted, and received power is measured at different positions, as illustrated in Fig. 16.

At θ_n=19°, the maximum received power is 58.07 W. Compared with the situation without the addition of the codirectional auxiliary coil, the received power has

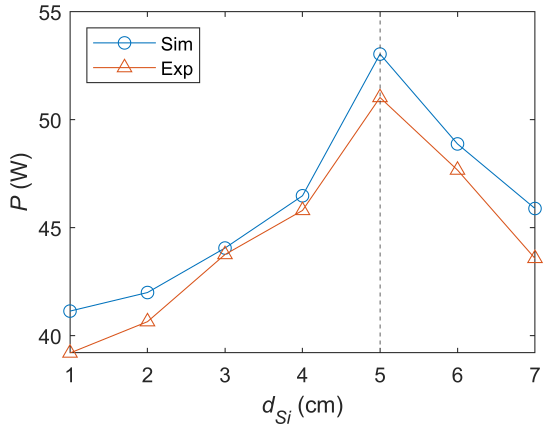

Fig. 15. The experiment results of received power with codirectional auxiliary coil.

Table 3: The experiment results of received power with codirectional auxiliary coil

d_{Si}	d_{Ri}	**Received Power**
1 cm	7 cm	39.2 W
2 cm	6 cm	40.65 W
3 cm	5 cm	43.76 W
4 cm	4 cm	45.8 W
5 cm	3 cm	51.03 W
6 cm	2 cm	47.67 W
7 cm	1 cm	43.58 W

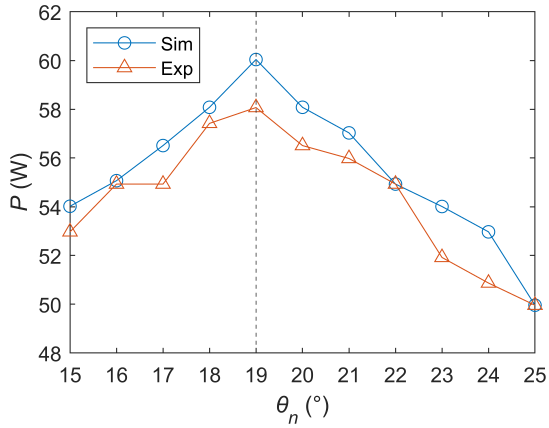

Fig. 16. The experiment results of received power with two auxiliary coils.

increased by 7.04 W. In comparison with the original two-coil system, the received power has increased by 14.92%.

When θ_n=19°, the transfer power is measured by varying the distance between the variable direction auxiliary coil and the receiving coil, as shown in Fig. 17. The power rapidly decreases when the variable direction auxiliary coil is located at other positions.

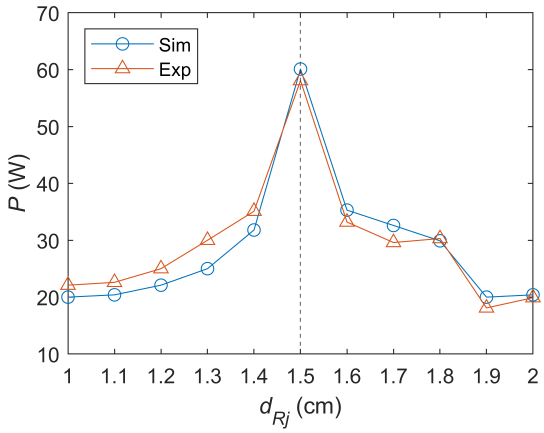

Fig. 17. The experiment results of received power with two auxiliary coils when θ_n=19°.

When L_i and L_j are not placed according to the proposed design method, even when operating at the resonant frequency, the power is lower. As shown in Fig. 18, at different distances, the power is consistently below 35 W.

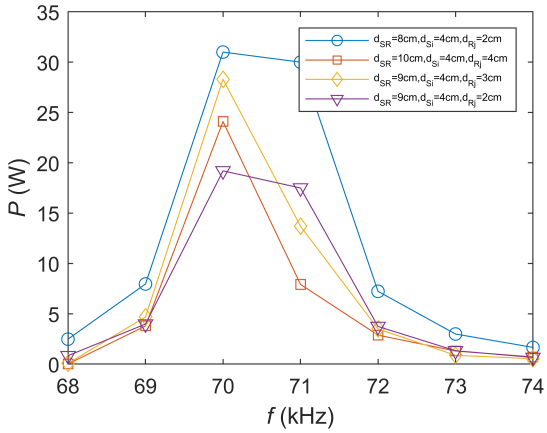

Fig. 18. Transfer power of coils at different positions.

The above experiment demonstrates that auxiliary coils can effectively enhance the received power of the system. The variable direction transfer method proposed in this paper proves effective in improving received power at specific positions. Consistency between the computational electromagnetics analysis and experimental results validated the feasibility of our design method.

V. CONCLUSION

In application scenarios, when the sending and receiving coils deviate from being parallel, the

performance of the WPT system deteriorates significantly. In traditional two-coil WPT systems, the received power experiences a considerable reduction when the receiving coil is rotated. Addressing this issue, this paper introduces a method for a variable direction WPT system based on two auxiliary coils.

Due to the lack of explicit formulas for calculating power in complex WPT systems, the mutual inductance and current related to transfer characteristics were analyzed. To validate the rationality of the design method, the magnetic flux distribution of the system was studied through simulations. Finally, the analysis results were verified through experiments, confirming the feasibility of the proposed approach.

Moreover, when altering the angle between the sending and receiving coils, the proposed variable direction transfer method also contributes to improved received power. Nonetheless, the transfer efficiency remains suboptimal, prompting further investigation into optimizing the coil structure and control modes as our next step. In other scenarios, adopting more coils and using intelligent algorithms to calculate parameters are also our future work.

ACKNOWLEDGMENT

This work was supported by Postgraduate Research & Practice Innovation Program of Jiangsu Province under Grant KYCX23_3091.

REFERENCES

[1] B. Sami and T. Mauro, "Theoretical study of different access points in coupled wireless power transfer - powerline communication systems," *Appl. Comput. Electromagn. Soc. J.*, vol. 33, no. 10, pp. 1112-1116, 2018.

[2] X. Huang, Y. Dou, S. Lin, Y. Tian, and M. Andersen, "Synchronous push-pull class E rectifiers with load-independent operation for megahertz wireless power transfer," *IEEE Trans. Power Electron.*, vol. 36, no. 6, pp. 6351-6363, 2020.

[3] D. Kim, A. T. Sutinjo, and A. Abu-Siada, "Near-field analysis and design of inductively-coupled wireless power transfer system in FEKO," *Appl. Comput. Electromagn. Soc. J.*, vol. 35, no. 1, pp. 82-93, 2020.

[4] S. Li and C. Mi, "Wireless power transfer for electric vehicle applications," *IEEE J. Em. Sel. Top. P.*, vol. 3, no. 1, pp. 4-17, 2015.

[5] Y. Gao, C. Duan, A. A. Oliveira, A. Ginart, K. B. Farley, and T. Zion, "Three-dimensional coil positioning based on magnetic sensing for wireless EV charging," *IEEE Trans. Transp. Electrification*, vol. 3, no. 3, pp. 578-588, 2017.

[6] X. Wu, P. Sun, S. Yang, L. He, and J. Cai, "Review on underwater wireless power transfer technology and its application," *Trans. China Electrotech. Soc.*, vol. 34, no. 8, pp. 1559-1568, 2019.

[7] R. Sasaki, K. Koizumi, and S. Kiryu, "Wireless power transmission with a sown auxiliary coil to improve power efficiency for an implantable device," *Int. J. Appl. Electron.*, vol. 64, no. 1-4, pp. 843-851, 2020.

[8] D. H. Sadek, H. A. Shawkey, and A. A. Zekry, "Multiband triple L-Arms patch antenna with diamond slot ground for 5G applications," *Appl. Comput. Electromagn. Soc. J.*, vol. 36, no. 3, pp. 302-307, 2021.

[9] H. Sun, S. Hou, Y. Zhao, W. Yan, and Y. Wu, "Investigation of electromagnetic exposure of WPT coil to human body based on biological electromagnetic safety assessment," *Appl. Comput. Electromagn. Soc. J.*, vol. 36, no. 10, pp. 1355-1366, 2021.

[10] H. Zhang, Z. Zhong, and W. Wu, "Adaptive compensation loop control method for dynamic range wireless power transfer in endoscopic capsules applications," *Appl. Comput. Electromagn. Soc. J.*, vol. 33, no. 5, pp. 499-504, 2018.

[11] A. Kurs, A. Karalis, R. Moffatt, J. D. Joannopoulos, P. Fisher, and M. Soljacic, "Wireless power transfer via strongly coupled magnetic resonances," *Science*, vol. 317, no. 5834, pp. 83-86, 2007.

[12] Y. Guo, L. Wang, and C. Liao, "A general equivalent model for multi-coil wireless power transfer system analysis and its application on compensation network design," *Appl. Comput. Electromagn. Soc. J.*, vol. 33, no. 6, pp. 648-656, 2018.

[13] A. K. Ranaweera, C. A. Moscoso, and J. W. Lee, "Anisotropic metamaterial for efficiency enhancement of mid-range wireless power transfer under coil misalignment," *J. Phys. D.*, vol. 48, no. 45, Art no. 455104, 2015.

[14] S. Wang, C. Jiang, X. Tao, F. Chen, C. Rong, C. Lu, Y. Zeng, X. Liu, R. Liu, and B. Wei, "Enhancing the stability of medium range and misalignment wireless power transfer system by negative magnetic metamaterials," *Materials*, vol. 13, no. 24, Art no. 5695, 2020.

[15] P. Yadav and M. Veerachary, "Auxiliary coil based square coupler for wireless power transfer system," *IEEE Trans. Ind. Appl.*, vol. 58, no. 4, pp. 4980-4993, 2022.

[16] X. Wang, C. Yu, Y. Wu, and J. Wang, "Structure design of quadrilateral overlapped wireless power transmission coupling coil," *Sensors*, vol. 22, no. 16, Art no. 5955, 2022.

[17] J. H. Cho, S. H. Jung, and Y. J. Kim, "Wireless power transfer for variable load, distance, and power division ratio in a loosely-coupled

multiple-receiver relay system," *IEEE Trans. Ind. Appl.*, vol. 70, no. 7, pp. 6809-6818, 2023.

[18] W. Tang, Q. Zhu, J. Yang, D. Song, and R. Zou, "Simultaneous 3-D wireless power transfer to multiple moving devices with different power demands," *IEEE Trans. Power Electron.*, vol. 35, no. 5, pp. 4533-4546, 2019.

[19] C. Liu, K. T. Chau, C. Qiu, and F. Lin, "Investigation of energy harvesting for magnetic sensor arrays on Mars by wireless power transmission," *J. Appl. Phys.*, vol. 115, no. 17, Art no. 17E702, 2014.

[20] A. Ali, N. Yasin, A. Rambe, I. Adam, N. Ramli, H. Rahim, T. Sabapathy, M. Norizan, and S. Sobri, "Analysis of symmetric two and four-coil magnetic resonant coupling wireless power transfer," *Appl. Comput. Electromagn. Soc. J.*, vol. 37, no. 4, pp. 497-506, 2022.

[21] S. Liu, Y. Feng, W. Weng, J. Chen, J. Wu, and X. He, "Contactless measurement of current and mutual inductance in wireless power transfer system based on sandwich structure," *IEEE Trans. Emerg.*, vol. 10, no. 5, pp. 6345-6357, 2022.

[22] X. Zhang, C. Xue, and J. Lin, "Distance-insensitive wireless power transfer using mixed electric and magnetic coupling for frequency splitting suppression," *IEEE Trans. Microw. Theory Tech.*, vol. 65, no. 11, pp. 4307-4313, 2017.

[23] Z. Liao, S. Ma, Q. Feng, C. Xia, and D. Yu, "Frequency splitting elimination and utilization in magnetic coupling wireless power transfer systems," *IEEE Trans. Circuits Syst. I Regul. Pap.*, vol. 68, no. 2, pp. 929-939, 2021.

Feihang Xiao received the B.S. degree in electrical engineering and automation from Changzhou University, China, in 2022. He is currently pursuing the M.S. degree with the School of Mechanical Engineering and Rail Transit, Changzhou University, China. His research interests include wireless power transfer and metamaterials.

Hao Qiang received the B.S. and M.S. degrees in electrical engineering from the Nanjing University of Science and Technology, Nanjing, China, in 2000 and 2004, respectively, and the Ph.D. degree in electrical engineering from Southeast University, China, in 2015. He was the Deputy Director of the Department of Electrical Engineering and Automation. Since 2007, he has been engaged in the teaching of electrical engineering and automation. His research interests include wireless power transfer, metamaterials, image processing, and vehicles to grid.